2024 IEEE International Workshop on Radio Frequency and Antenna Technologies (iWRF&AT) | 979-8-3503-8476-5/24/$31.00 ©2024 IEEE | DOI: 10.1109/iWRFAT61200.2024.10594363

Energy Consumption Minimization for UAV-Mounted Active RIS-Assisted Mobile Edge Computing

Jiabin Shuai[1], Yejun He[1,*], Xiaowen Cao[1], and Lifeng Xie[2]
[1]State Key Laboratory of Radio Frequency Heterogeneous Integration
Sino-British Antennas and Propagation Joint Laboratory, Ministry of Science and Technology of China
Guangdong Engineering Research Center of Base Station Antennas and Propagation
Shenzhen Key Laboratory of Antennas and Propagation
College of Electronics and Information Engineering, Shenzhen University, 518060, China
[2] Department of Broadband Communication, Peng Cheng Laboratory, Shenzhen, China
Email: 2659095556@qq.com, heyejun@126.com*, caoxwen@szu.edu.cn, xielf@pcl.ac.cn

***Abstract*—In this paper, we propose a UAV-mounted active reconfiguration intelligent surface (U-ARIS)-assisted mobile edge computing (MEC) system, where multiple users transmit data to the edge server with the assistance of an U-ARIS. Our goal is to minimize the overall energy consumption (EC) by jointly optimizing the UAV trajectory and amplification/reflection coefficients of the ARIS. Due to the highly coupled optimization variables, the formulated problem is non-convex and hard to be optimally solved. To address these challenges, we leveraged the block coordinate descent (BCD) and successive convex approximation (SCA) algorithm to iteratively solve the original problem for obtaining a local optimum. Numerical results demonstrate that the proposed algorithm can significantly reduce the EC of the U-ARIS-assisted MEC system when compared to other benchmark solutions.**

***Index Terms*—Active reconfiguration intelligent surface, mobile edge computing, unmanned aerial vehicle, block coordinate descent.**

I. Introduction

Mobile edge computing (MEC) has emerged as a prospective solution to facilitate ultra-reliable low-latency communication for a myriad of real-time processing and mission-critical applications, encompassing domains such as autonomous driving, a diverse range of Internet of Things (IoT) devices, remote surgery, and industrial automation [1]- [3]. The main feature of MEC is to decentralize mobile computing, network control, and storage by pushing them to the network edges. This approach aims to bring computing resources closer to the end-user terminals, resulting in a significant reduction in communication latency [4]- [6]. However, for those devices in remote areas with a lack of robust and reliable network connectivity, it poses challenges in establishing and maintaining communication links to provide seamless MEC services.

Towards this end, reconfigurable intelligence surface (RIS) has been considered as a cutting-edge technology to enhance wireless networks communication capabilities, owing to the capability to create a more favorable propagation environment [7] [8]. RIS can be broadly categorized into active and passive types based on their functionalities, namely the passive RIS and active RIS (ARIS). Unlike that the former consisting of reflective surfaces or metamaterial elements has a fixed configuration and cannot dynamically adapt to changing conditions, ARIS incorporating adjustable phase shifters can actively modify its configuration based on the requirements of the communication system [9]- [10]. A hybrid RIS/ARIS was proposed by the authors in [11]. This RIS combines both active and passive reflecting elements. In [12], an ARIS was incorporated into a single-user single-input multi-output system with the aim of improving the signal-to-noise ratio for the user.

The introduction of UAVs enhances the mobility and flexibility of RIS, enabling it to better adapt to complex and dynamic communication environments, ultimately improving the performance and efficiency of communication systems. In [13], the authors investigated a UAV-MEC system that utilizes time division multiple access (TDMA) to improve system performance by optimizing both the UAV and computation resources. Moreover, the works in [14] discussed a RIS-asissted UAV system and aimed to optimize the UAV's data transfer rate while simultaneously minimizing the energy expended on UAV propulsion. However, the UAV-RIS-assisted MEC system discussed in the aforementioned papers still faces challenges associated with double effect. The application of UAV-RIS in MEC is relatively scarce in current research, thus motivates our work.

In this paper, we propose a MEC system assisted by a U-ARIS. The objective is to minimize the total energy consumption (EC) through the joint optimization of the UAV trajectory and the amplification/reflection coefficients of the ARIS. Given the strong coupling among optimiza-

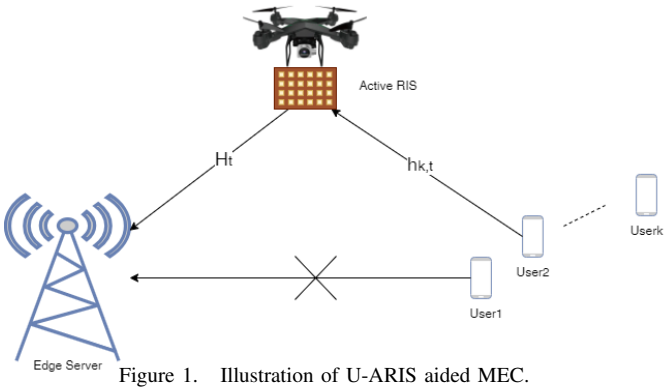

Figure 1. Illustration of U-ARIS aided MEC.

tion variables, the formulated problem is non-convex and challenging to solve optimally. To address this, we propose an algorithm based on block coordinate descent (BCD) and successive convex approximation (SCA). The simulation results validate that our proposed model achieves superior performance.

II. System Model and Problem Formulation

In this paper, we propose a U-ARIS-asissted MEC system as shown in Fig. 1. The U-ARIS system involves serving K single-antenna users, allowing them to offload computation tasks to the MEC server which is equipped with N antennas. The U-ARIS itself is equipped with M reflecting elements, enabling the reconfiguration of the propagation environment and enhancement of the quality of reflected signals. To ease of exposition, the set of users are denoted by $k \in \mathcal{K} \triangleq \{1, 2, ..., K\}$. The reflection elements of ARIS are indexed by $m \in \mathcal{M} \triangleq \{1, 2, ..., M\}$. The mission period is discretized into T time slots with size of δ_t and indexed by $t \in \mathcal{T} \triangleq \{1, 2, ..., T\}$.

A. U-ARIS assisted MEC system

Suppose that the MEC server and each user $k \in \mathcal{K}$ are located at fixed locations on the ground in a three-dimensional (3D) Cartesian coordinate system, which the horizontal coordinate is given $\mathbf{w}_s = [w_{s,1}, w_{s,2}]$ and $\mathbf{w}_k = [w_{k,1}, w_{k,2}]$, respectively. We assume that the U-ARIS remains at a constant altitude denoted by H and its position remains fixed throughout each time slot. Therefore, the U-ARIS's horizontal trajectory and speed during time slot t can be expressed using the sequence as $\mathbf{q}_t = [x_t, y_t], \mathbf{v}_t = [v_{t,1}, v_{t,2}], t \in \mathcal{T}$, adhering to the following mechanical and flight limitations

$$\mathbf{q}_1 = \mathbf{q}_0, \mathbf{q}_{T+1} = \mathbf{q}_F, |x_t| \leq r_1, |y_t| \leq r_2, \forall t \quad (1)$$

$$\|\mathbf{v}_t\| \leqslant v_{max}, \forall t \quad (2)$$

$$\mathbf{q}_{t+1} = \mathbf{q}_t + \mathbf{v}_t \delta_t, \forall t, \quad (3)$$

where v_{max} is the UAVs maximum speed, $\mathbf{q}_0$ and $\mathbf{q}_F$ denote the initial and final positions of the U-ARIS, and r_1, r_2 are the horizontal flight range of the U-ARIS.

The baseband equivalent channels during time slot t are denoted as $\mathbf{H}_t \in \mathbb{C}^{N \times M}$ for the U-ARIS to MEC server link, and $\mathbf{h}_{k,t} \in \mathbb{C}^{M \times 1}$ for the k-th user to U-ARIS link. We are examining the TDMA scheme for task offloading. The communication time for each user during the t-th slot remains the same, i.e., $\frac{\delta_t}{K}$.

The amplitude and phase of the m-th element for k-th user during t-th time slot on ARIS are denoted as $\beta_{k,t,m}$ and $\theta_{k,t,m} \in [0, 2\pi)$, respectively, let $\mathbf{\Theta}_{k,t} = diag(\beta_{k,t,1} e^{j\theta_{k,t,1}}, \cdots, \beta_{k,t,M} e^{j\theta_{k,t,M}})$. In contrast to passive RISs, ARISs are designed with individual amplifiers associated with their reflecting elements, which consume extra power. Consequently, the thermal noise at the ARIS cannot be disregarded. As a result, the signal received at the MEC server during time slot t is represented as follow

$$\mathbf{y}_t = \sqrt{p}\mathbf{H}_t \mathbf{\Theta}_{k,t} \mathbf{h}_{k,t} s_{k,t} + \mathbf{H}_t \mathbf{\Theta}_{k,t} \mathbf{u}_t + \mathbf{n}_t, \quad (4)$$

where $s_{k,t}$ and p represent the data symbol transmitted by the user and the associated transmit power during time slot t, and $\mathbf{u}_t \in \mathbb{C}^{M \times 1} \sim \mathcal{CN}(\mathbf{0}_M, \sigma_h^2 \mathbf{I}_M)$ and $\mathbf{n}_t \in \mathbb{C}^{N \times 1} \sim \mathcal{CN}(\mathbf{0}_N, \sigma^2 \mathbf{I}_N)$ denote the thermal noise at the U-ARIS and the MEC server during time slot t, respectively. It is assumed that each $s_{k,t} \sim \mathcal{CN}(0, 1)$ for $\forall k \in \mathcal{K}$. For simplicity, the MEC server-U-ARIS and U-ARIS-user channels are all modeled as Rician channel.

B. Delay

We make the assumption that the MEC server employs linear receive beamforming for signal decoding. By representing $\mathbf{F}_t = [\mathbf{f}_{1,t}, \cdots, \mathbf{f}_{K,t}] \in \mathbb{C}^{N \times K}$ as the collection of receiving beamforming vectors during time slot t, the signal recovered at the MEC server during time slot t is expressed as follow

$$\widehat{\mathbf{s}}_t = \mathbf{F}_t^H \mathbf{y}_t, \quad (5)$$

where $\widehat{\mathbf{s}}_t = [\widehat{s}_{1,t}, \cdots, \widehat{s}_{K,t}]^T$ and $\widehat{s}_{k,t}$ is the recovered signal for the k-th user during time slot t and $(\cdot)^H$ denotes conjugate transpose operations.

Then, the achievable computation offloading rate (bits/s/Hz) of the k-th user during time slot t is given by

$$R_{k,t} = \log_2 (1 + \gamma_{k,t}), \quad (6)$$

and

$$\gamma_{k,t} = \frac{p \left| \mathbf{f}_{k,t}^H \mathbf{G}_{k,t} \mathbf{h}_{k,t} \right|^2}{\sigma_h^2 \left\| \mathbf{f}_{k,t}^H \mathbf{G}_{k,t} \right\|^2 + \sigma^2 \left\| \mathbf{f}_{k,t}^H \right\|^2}, \quad (7)$$

where $\mathbf{G}_{k,t} = \mathbf{H}_t \mathbf{\Theta}_{k,t}$. The linear minimum-mean-square-error (MMSE) detector is recognized as the optimal receive beamforming for any given reflecting coefficient matrix $\mathbf{\Theta}_{k,t}$ and $\mathbf{q}_t$. This is particularly advantageous in handling elevated interference resulting from the active RIS noise amplification. The expression for the MMSE-based receive beamforming is as follow

$$\mathbf{f}_{k,t}^* = \frac{\left(\mathbf{\Lambda}_{k,t} \mathbf{\Lambda}_{k,t}^H + \frac{\sigma_h^2}{p} \mathbf{G}_{k,t} \mathbf{G}_{k,t}^H + \frac{\sigma^2}{p} \mathbf{I}_N \right)^{-1} \mathbf{\Lambda}_{k,t}}{\left\| \left(\mathbf{\Lambda}_{k,t} \mathbf{\Lambda}_{k,t}^H + \frac{\sigma_h^2}{p} \mathbf{G}_{k,t} \mathbf{G}_{k,t}^H + \frac{\sigma^2}{p} \mathbf{I}_N \right)^{-1} \mathbf{\Lambda}_{k,t} \right\|}, \quad (8)$$

where $\mathbf{\Lambda}_{k,t} = \mathbf{G}_{k,t}\mathbf{h}_{k,t}$.

Our research focuses on exploring a partial offloading scheme utilizing the data-partition model. In this particular model, it is assumed that the task-input bits are independent at the bit level. To facilitate the offloading process, each user divides its computational task into two segments, one segment is processed locally, while the other segment of the computational task is offloaded to the MEC server. The computational task for the U-ARIS-assisted MEC system under consideration is elaborated as follow

1) Local computing: For the k-th user during the t-th time slot, the number of bits for local computation and the number of bits for offloading can be represented as $l^l_{k,t}$ and $l^o_{k,t}$, respectively. The local computational task by the k-th user due to local computing during time slot t can be constrained as follow

$$l^l_{k,t} \leqslant \frac{\delta_t f_L}{Kc}, \tag{9}$$

where f_L denotes the local computing resource and c is the number of CPU cycles required to process each bit.

2) Task offloading: Compared to the offloaded computational task, the size of the computational result is typically much smaller, resulting in a negligible feedback delay. Therefore, the offloaded computational task for the k-th user during t-th time slot is primarily determined as

$$l^o_{k,t} \leqslant \frac{\delta_t R_{k,t}}{K}. \tag{10}$$

It is assumed that the users simultaneously perform both local computing and computation offloading. We have the following

$$l_{k,t} = (l^o_{k,t} + l^l_{k,t}), \forall k, t. \tag{11}$$

C. Energy Consumption

In this paper, the EC of the U-ARIS-assisted MEC system is primarily composed of the following three components

1) The EC locally during time slot t can be formulated as

$$E_{L,t} = \sum_{k=1}^{K}(\frac{\delta_t}{K}p + \alpha_l l^l_{k,t} c f_L^2), \tag{12}$$

where α_l denotes the switched capacitance coeffient for the users.

2) The EC of the MEC sever can be denoted as

$$E_{E,t} = \sum_{k=1}^{K}\alpha_E l^o_{k,t} c f_E^2, \tag{13}$$

where α_E denotes the coeffient for the MEC server and f_E (cycle/s) is the edge computing resource.

3) The power consumption of the m-th element during time slot t can be derived as

$$P_{\mathrm{ARIS},t,m} = \xi p_{\mathrm{out},t,m} + P_{\mathrm{c}} + P_{\mathrm{DC}}, \tag{14}$$

where $\xi \triangleq \mu^{-1}$ with $\mu \in (0,1]$ being the amplifier efficiency, P_{DC} and P_{c} are the direct current biasing power consumption, the circuit power consumption of the ARIS, and $p_{\mathrm{out},t,m}$ is the output power of the m-th element of the ARIS which is related to the incident signal power $p_{\mathrm{in},t,m}$ during the t-th time slot in the form of

$$p_{\mathrm{out},t,m} = p_{\mathrm{in},t,m}|\beta_{k,t,m}e^{j\theta_{k,t,m}}|^2, \tag{15}$$

and $p_{\mathrm{in},t,m} = \sum_{k=1}^{K} p|h_{k,t,m}|^2 + \sigma^2$, $h_{k,t,m}$ denotes the channel from the k-th user to the m-th element of ARIS during the t-th time slot.

Therefore, we can get the EC of the ARIS during the t-th time slot as follow

$$E_{R,t} = \xi\sum_{k=1}^{K}(p\frac{\delta_t}{K}\left\|\mathbf{\Theta}_{k,t}\mathbf{h}_{k,t}\right\|^2 + \frac{\delta_t}{K}\left\|\mathbf{\Theta}_{k,t}\right\|^2\sigma_h^2) + M\delta_t(P_{\mathrm{c}} + P_{\mathrm{DC}}) \tag{16}$$

4) We utilize a novel EC model for rotary- wing UAVs according to [15], which accounts for the real- world thrust-to-weight ratio.

$$E_{p,t} = P_0\Big(1 + \frac{3\|\mathbf{v}_t\|^2}{U_{tip}^2}\Big) + \frac{1}{2}d_0\rho s A\|\mathbf{v}_t\|^3 + P_i\sqrt{(1 + \frac{\|\mathbf{v}_t\|^4}{4v_0^4})^{\frac{1}{2}} - \frac{\|\mathbf{v}_t\|^2}{2v_0^2}}, \forall t, \tag{17}$$

where $E_{\mathrm{p,t}}$ is the EC caused by the U-ARIS flight during time slot t. P_0, U_{tip}^2, d_0, ρ, A, v_0, s and P_i represent various mechanical coefficients associated with the EC model.

Hence, the average long-term EC of the system can be calculated using the following equation

$$E_{sum} = \sum_{t=1}^{T}(E_{R,t} + E_{L,t} + E_{E,t} + \iota E_{p,t}), \tag{18}$$

where ι represents the energy coefficient of UAV EC.

D. Problem Formulation

The overall problem of energy minimization for the case is formulated as follow

$$(P1): \min_{\mathbf{l},\mathbf{Q},\mathbf{v},\mathbf{\Theta}} E_{sum} \tag{19}$$

$$s.t. \quad \sum_{t=1}^{T} l_{k,t} + l^o_{k,t} \geqslant L_k, k \in \mathcal{K}, t \in \mathcal{T}, \tag{19a}$$

$$(1) - (3), (9), (10).$$

The computation volume is denoted as $\mathbf{l} \triangleq \{l^l_{k,t}, l^o_{k,t}, k \in \mathcal{K}, t \in \mathcal{T}\}$.

III. SOLUTION TO THE FORMULATED PROBLEM

In this section, we propose an effective algorithm based on the BCD method to solve the EC minimization problem (P1). The algorithm optimizes the variables alternately to achieve the desired objective.

A. Optimizing the computation volum $\mathbf{l}$

The subproblem for the computation volum design as follow

$$(P2): \min_{\mathbf{l}} \sum_{t=1}^{T}\sum_{k=1}^{K}(\alpha_l l^l_{k,t} c f_L^2 + \alpha_E l^o_{k,t} c f_E^2)$$

$$s.t. \quad (19a), (9), (10).$$

Problem (P2) is a convex optimization problem, which means it can be efficiently solved using standard convex optimization solvers.

B. Optimizing the reflect coffients $\mathbf{\Theta}$

The subproblem for the reflect coffients design as follow

$$(P3): \min_{\mathbf{\Theta}} \quad E_R$$
$$s.t. \quad (10)$$

where $E_R = \sum_{t=1}^{T} \xi \sum_{k=1}^{K} (p\frac{\delta_t}{K} \sum_{m=1}^{M} \beta_{k,t,m}^2 |h_{k,t,m}|^2 + \frac{\delta_t}{K} \sum_{m=1}^{M} \beta_{k,t,m}^2 \sigma_h^2)$

We can observe that the optimal phase shift of the ARIS can be represented as follow

$$\theta_{k,t,m}^* = -\arg(g_{k,t,m} h_{k,t,m}), \tag{20}$$

where $\mathbf{g}_{k,t} = [g_{k,t,1}, \cdots, g_{k,t,M}] = \mathbf{f}_{k,t}^H \mathbf{H}_t$. Therefore, constraint (10) can be reformulated as

$$\log_2 \left(1 + \frac{p(\sum_{m=1}^{M} \beta_{k,t,m} |g_{k,t,m} h_{k,t,m}|)^2}{\sigma_h^2 \sum_{m=1}^{M} \beta_{k,t,m}^2 |g_{k,t,m}|^2 + \sigma^2 \|f_{k,t}^H\|^2}\right) \geqslant \frac{l_{k,t}^o K}{\delta_t}, \tag{21}$$

and it can be reformulated as

$$(\sum_{m=1}^{M} \beta_{k,t,m} |g_{k,t,m} h_{k,t,m}|)^2 \geqslant \frac{2^{\frac{l_{k,t}^o K}{\delta_t}} - 1}{p} (\sigma_h^2 \sum_{m=1}^{M} \beta_{k,t,m}^2 |g_{k,t,m}|^2 + \sigma^2 \sum_{m=1}^{M} |f_{k,t,m}^H|^2), \quad \forall m \in \mathcal{M}, \forall k \in \mathcal{K}, \forall t \in \mathcal{T}. \tag{22}$$

To handle the non-convex constraint (22), we propose an algorithm based on SCA. This algorithm operates iteratively, approximating the constraint (22) at each iteration to obtain a locally optimal solution. Particularly, let $\beta_{k,t,m}^{(0)}, \forall m \in \mathcal{M}, \forall k \in \mathcal{K}, \forall t \in \mathcal{T}$ denote the initial coffient of ARIS and $\beta_{k,t,m}^{(i)}, \forall m \in \mathcal{M}, \forall k \in \mathcal{K}, \forall t \in \mathcal{T}$ the obtained coffients of ARIS after iteration $i \geqslant 1$. We have

$$(\sum_{m=1}^{M} \beta_{k,t,m}^{(i)} |g_{k,t,m} h_{k,t,m}|)^2 + 2 \sum_{m=1}^{M} |g_{k,t,m} h_{k,t,m}| (\beta_{k,t,m} - \beta_{k,t,m}^{(i)}) \geqslant \frac{2^{\frac{l_{k,t}^o K}{\delta_t}} - 1}{p} (\sigma_h^2 \sum_{m=1}^{M} \beta_{k,t,m}^2 |g_{k,t,m}|^2 + \sigma^2 \sum_{m=1}^{M} |f_{k,t,m}^H|^2). \tag{23}$$

Therefore, problem (P3) can be reformulated as

$$(P3.1): \min_{\mathbf{\Theta}} \quad E_R$$
$$s.t. \quad (23).$$

Therefore, problem (P3.1) can be transformed into a convex optimization problem, making it efficiently solvable using standard solvers. The detailed optimization procedure for determining the U-ARIS's phase shift is outlined in algorithm 1.

Algorithm 1 Proposed algorithm for solving problem P3.1

Initialize iterative number $i = 1$.
for $i \leqslant i_{max}$ and $\frac{|E_R^{(i+1)} - E_R^{(i)}|}{E_R^{(i+1)}} \geqslant \epsilon$ **do**
  Solve the convex problem (P3.1) to obtain $\mathbf{\Theta}_{k,t}^{(\eta)}$
  Update the iterative index $i = i + 1$.
end for
Output: phase shift $\mathbf{\Theta}_{k,t}^{(\eta)}$.

C. Optimizing the UAV trajectory and speed $\mathbf{Q}, \mathbf{v}$

The subproblem for the UAV trajectory design is as follow

$$(P4): \min_{\mathbf{Q},\mathbf{v}} \sum_{t=1}^{T} \xi \sum_{k=1}^{K} p\frac{\delta_t}{K} \|\mathbf{\Theta}_{k,t} \mathbf{h}_{k,t}\|^2 + \sum_{t=1}^{T} \iota E_{p,t}$$
$$s.t. \quad (1) - (3), (10).$$

To address the non-convex constraint (10), we propose an algorithm based on SCA. This algorithm operates iteratively, approximating the constraint (10) at each iteration to obtain a locally optimal solution. Particularly, let $\mathbf{q}_t^{(0)} = (x_t^{(0)}, y_t^{(0)}), \forall t \in \mathcal{T}$ denote the initial trajectory and $\mathbf{q}_t^{(j)} = (x_t^{(j)}, y_t^{(j)}), \forall t \in \mathcal{T}$ denote the obtained trajectory after iteration $j \geqslant 1$. We have

$$A_{k,t} + \frac{B_{k,t}}{\ln 2 A_{k,t}} (x_t - x_t^{(j)}) + \frac{C_{k,t}}{\ln 2 A_{k,t}} (y_t - y_t^{(j)}) \geqslant \frac{l_{k,t}^o K}{\delta_t}. \tag{24}$$

where

$$A_{k,t} = 1 + \frac{\frac{e_{k,t}^1}{(d_{H,t}^{(j)})^2 (d_{h,k,t}^{(j)})^2}}{\frac{e_{k,t}^2}{(d_{H,t}^{(j)})^2} + \sigma^2 \|\mathbf{f}_{k,t}^H\|^2}$$
$$B_{k,t} = -\frac{e_{k,t}^1 (e_{k,t}^2 O_{k,t}^{(j)} + \sigma^2 \|\mathbf{f}_{k,t}^H\|^2 \Gamma_{k,t}^{(j)})}{(e_{k,t}^2 (d_{h,k,t}^{(j)})^2 + \sigma^2 \|\mathbf{f}_{k,t}^H\|^2 (d_{H,t}^{(j)})^2 (d_{h,k,t}^{(j)})^2)^2}$$
$$C_{k,t} = -\frac{e_{k,t}^1 (e_{k,t}^2 \Omega_{k,t}^{(j)} + \sigma^2 \|\mathbf{f}_{k,t}^H\|^2 \Pi_{k,t}^{(j)})}{(e_{k,t}^2 (d_{h,k,t}^{(j)})^2 + \sigma^2 \|\mathbf{f}_{k,t}^H\|^2 (d_{H,t}^{(j)})^2 (d_{h,k,t}^{(j)})^2)^2}, \tag{25}$$

and

$$\Gamma_{k,t}^{(j)} = 2(x_t^{(j)} - w_{s,1})(d_{h,k,t}^{(j)})^2 + 2(x_t^{(j)} - w_{k,1})(d_{H,t}^{(j)})^2$$
$$\Pi_{k,t}^{(j)} = 2(y_t^{(j)} - w_{s,2})(d_{h,k,t}^{(j)})^2 + 2(y_t^{(j)} - w_{k,2})(d_{H,t}^{(j)})^2$$
$$O_{k,t}^{(j)} = 2(x_t^{(j)} - w_{k,1})$$
$$\Omega_{k,t}^{(j)} = 2(y_t^{(j)} - w_{k,2})$$
$$e_{k,t}^1 = p| \sum_{m=1}^{M} \sum_{n=1}^{N} f_{k,t,n}^H H_{t,n,m}^{'} \Theta_{k,t,m} h_{k,t,m}^{'}|^2$$
$$e_{k,t}^2 = \sigma_h^2 \sum_{m=1}^{M} |\sum_{n=1}^{N} f_{k,t,n}^H H_{t,n,m}^{'} \Theta_{k,t,m}|^2, \tag{26}$$

and

$$H_{t,n,m}^{'} = \frac{H_{t,n,m}}{d_{H,t}}, h_{k,t,m}^{'} = \frac{h_{k,t,m}}{d_{h,k,t}}$$
$$d_{h,k,t}^{(j)} = \|\mathbf{q}_t^{(j)} - \mathbf{w}_k\|, d_{H,t}^{(j)} = \|\mathbf{q}_t^{(j)} - \mathbf{w}_s\|. \quad (27)$$

We successively apply the inequality $(a^2+b^2)^{\frac{1}{2}} \leqslant (a+b), a, b \in \mathbb{R}_+$ for $E_{p,t}$. Therefore, we obtain a convex upper bound of $E_{p,t}$, which can be expressed as follow

$$E_{up,t} = P_0\Big(1 + \frac{3\|\mathbf{v}_t\|^2}{U_{tip}^2}\Big) + \frac{1}{2}d_0\rho s A\|\mathbf{v}_t\|^3 + P_i, \forall t, \quad (28)$$

after the above operations, problem (P5) can be reformulated as

$$(P4.1): \min_{\mathbf{Q},\mathbf{v}} \sum_{t=1}^{T}\xi\sum_{k=1}^{K}p\frac{\delta_t}{K}\frac{\sum_{m=1}^{M}|\theta_{k,t,m}h_{k,t,m}^{'}|^2}{d_{h,k,t}^2} + \sum_{t=1}^{T}\iota E_{up,t}$$
$$s.t. \quad (1)-(3), (24).$$

Then, we reformulate (P4.1) by introducing slack variable $\omega_{k,t} \leqslant d_{h,k,t}^2$ as

$$(P4.2): \min_{\mathbf{Q},\mathbf{v},\omega} \sum_{t=1}^{T}\xi\sum_{k=1}^{K}p\frac{\delta_t}{K}\frac{\sum_{m=1}^{M}|\theta_{k,t,m}h_{k,t,m}^{'}|^2}{\omega_{k,t}} + \sum_{t=1}^{T}\iota E_{up,t}$$
$$s.t. \quad d_{h,k,t}^{2,(j)} + 2(\mathbf{q}_t^{(j)} - \mathbf{w}_k)(\mathbf{q}_t - \mathbf{q}_t^{(j)})^T \geqslant \omega_{k,t}, \quad (29)$$
$$(1)-(3), (24).$$

Problem (P4.2) is a convex optimization problem, which means it can be efficiently solved using standard solvers for convex optimization problems. Derived from the solutions acquired in the preceding subsections, the algorithm steps are similar to algorithm 1, so we don't go into further detail here.

Below is the summary of the proposed BCD algorithm for solving problem (P1), as outlined in algorithm 2.

Algorithm 2 BCD algorithm for solving problem P1

Initialize iterative number $\eta = 1$.
for $\eta \leqslant \eta_{max}$ and $\frac{|E_{sum}^{(\eta+1)} - E_{sum}^{(\eta)}|}{E_{sum}^{(\eta+1)}} \geqslant \epsilon$ **do**
  Solve problem (P2) to obtain $l_{k,t}^{l,(\eta)}$ and $l_{k,t}^{o,(\eta)}$ for given $\mathbf{\Theta}_{k,t}$ and $\mathbf{q}_t, \mathbf{v}_t$.
  Solve problem (P3.1) to obtain $\mathbf{\Theta}_{k,t}^{(\eta)}$ according to the updated $l_{k,t}^{l,(\eta)}$, $l_{k,t}^{o,(\eta)}$ and given $\mathbf{q}_t, \mathbf{v}_t$.
  Solve problem (P4.2) to obtain $\mathbf{q}_t^{(\eta)}, \mathbf{v}_t^{(\eta)}$ according to the updated $l_{k,t}^{l,(\eta)}$, $l_{k,t}^{o,(\eta)}$ and $\mathbf{\Theta}_{k,t}^{(\eta)}$.
  Calculate $E_{sum}^{(\eta)}$.
  Update the iterative index $\eta = \eta + 1$.
end for
Output: the optimal bit allocation $l_{k,t}^{l*}$, $l_{k,t}^{o*}$, phase shift $\mathbf{\Theta}_{k,t}^{*}$, and UAV trajectory $\mathbf{q}_t^{*}, \mathbf{v}_t^{*}$.

IV. Simulation Result

In this section, we conduct simulations to validate the proposed algorithm in the context of the U-ARIS-assisted MEC system. We compare the numerical results with benchmark systems to evaluate their performance, including one that operates on a UAV with fixed ARIS, one that operates with fixed trajectory and another that operates on a UAV with random ARIS.

In the simulation setup, the positions of the U-ARIS and MEC-server are configured as (500 m, 0 m) and (0 m, 0 m), respectively. Four users with the same computation offloading power are randomly distributed within a 1000 m 1000 m region. The heights of the users, U-ARIS, and MEC server are specified as 0 m, 50 m, and 0 m, respectively. The other simulation parameters for the U-ARIS-assisted MEC system are outlined in Table I. For simplicity, the MEC

Table I
PARAMETER SETTINGS ON SIMULATION

parameter	value
Bandwidth B, transmit power p	1 MHz, 0.5 W
U_{tip}, v_0, d_0, s, ρ, G	$120, \sqrt{\frac{20}{2*1.225*0.503}}, 0.6, 0.05, 1.225, 0.503$
P_0, P_i	$\frac{0.012*120^3}{8}\rho s G, \frac{1.1*20^{3/2}}{\sqrt{2\rho G}}$
M, N;	16,4
σ_{h}^2, σ^2	-60 dBm,-70 dBm
T,δ_t, v_{max}	100,1 s,50 m/s
ι	0.001
f_E, f_L, c	$5*10^8$,$50*10^9$,1000
ξ, r_1, r_2	$1.25, 500, 500$

server-U-ARIS channel is modeled as Rician channel,

$$\mathbf{H}_t = \sqrt{\frac{\tau D_t}{1+\tau}}\bar{\mathbf{H}}_t + \sqrt{\frac{D_t}{1+\tau}}\tilde{\mathbf{H}}_t, \quad (30)$$

where $\tilde{\mathbf{H}}_t$ is NLoS component during time slot t, and each element of $\tilde{\mathbf{H}}_t$ is complex gaussian distributed with zero mean and unit variance; τ is the Rician factor and $\bar{\mathbf{H}}_t$ is LoS component during time slot t. In this paper, we make the assumption that the channel state information (CSI) for the MEC server-U-ARIS and U-ARIS-UE channels is available. This information can be obtained through various existing channel estimation techniques.

According to distance-dependent loss model, the large-scale path loss is denoted as $D_t = D_0\left(\frac{d_{H,t}}{d_0}\right)^{-\kappa_1}$, and $\kappa_1 = 2$ is the path loss exponent and $d_{H,t} = \sqrt{H^2 + (x_t - x_s)^2 + (y_t - y_s)^2}$ is the distance between the MEC server and the U-ARIS.

Figure 2 shows the U-ARIS trajectory onto the horizontal plane when $L = 10$ Mbits, $p = 0.5$ W. Observations from Fig. 2 indicates that on the one hand, UAV will move away from users to minimize energy consumption and on the other hand, UAV will not go too far from users to meet the constraints of user reachability. Figure 3 depicts the correlation between energy consumption and the task of processing data bits when $p = 0.5$ W, comparing scenarios

involving fixed ARIS, fixed trajectory, and active RIS with random phase shifts. As the task of processing data bits increases, energy consumption will also increase. Notably, the figure highlights that, the energy consumption of ARIS remains lower. ARIS proves to be a highly effective solution for addressing the challenges posed by double path loss attenuation in wireless communication systems. Its compact size and flexible deployment options further enhance its applicability in various environments.

Figure 4 depicts the correlation between energy consumption and user transmit power when $L = 10$ Mbits. With the increase in user transmission power, the total energy consumption also increases. It is easy to observe that ARIS exhibits lower total energy consumption compared to other benchmark system.

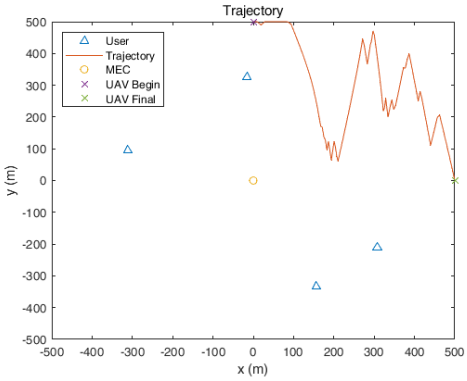

Figure 2. Trajectory

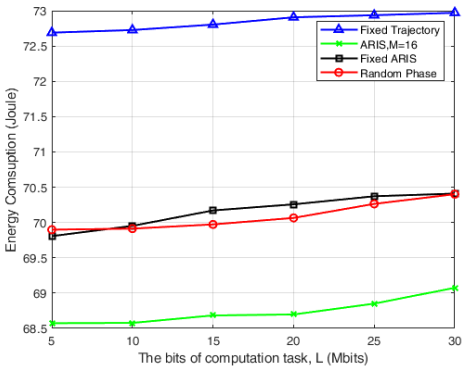

Figure 3. Energy consumption versus the bits of computation task.

V. Conclusion

In this paper, we proposed the U-ARIS-assisted MEC system to reduce the energy comsuption. A joint optimization algorithm based on BCD and SCA had been proposed to solve the problem of minimizing system energy consumption. Simulation results indicated that ARIS has better performance, resulting in reduced overall system energy consumption.

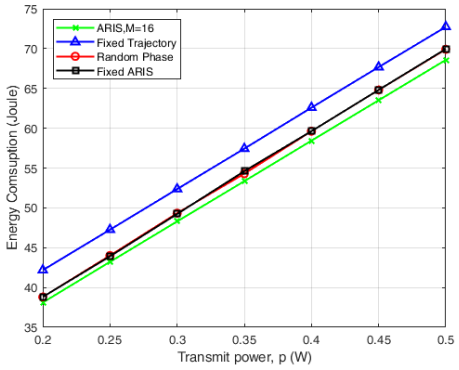

Figure 4. Energy consumption versus the user transmit power.

References

[1] Y. Wang, M. Chen, Z. Li and Y. Hu, "Joint allocations of radio and computational resource for user energy consumption minimization under latency constraints in multi-cell MEC systems," *IEEE Trans. Veh. Technol.*, vol. 72, no. 3, pp. 3304-3320, Mar. 2023.

[2] C. -F. Liu, M. Bennis, M. Debbah, and H. V. Poor, "Dynamic Task Offloading and Resource Allocation for Ultra-Reliable Low-Latency Edge Computing," *IEEE Trans. Commun.*, vol. 67, no. 6, pp. 4132-4150, Jun. 2019.

[3] Y. Yang, Y. Hu, and M. C. Gursoy, "Energy efficiency analysis in RISaided MEC networks with finite blocklength codes," in *Proc. IEEE WCNC*, Apr. 2022, pp. 423428.

[4] Y. Mao, C. You, J. Zhang, K. Huang, and K. B. Letaief, "A survey on mobile edge computing: The communication perspective," *IEEE Commun. Surveys Tuts.*, vol. 19, no. 4, pp. 2322-2358, Aug. 2017.

[5] W. Shi, J. Cao, Q. Zhang, Y. Li, and L. Xu, "Edge computing: Vision and challenges," *IEEE Internet Things J.*, vol. 3, no. 5, pp. 637-646, Oct. 2016.

[6] X. Cao, F. Wang, J. Xu, R. Zhang and S. Cui, "Joint Computation and Communication Cooperation for Energy-Efficient Mobile Edge Computing," *IEEE Internet Things J.*, vol. 6, no. 3, pp. 4188-4200, Jun. 2019.

[7] B. Duo, M. He, Q. Wu, and Z. Zhang, "Joint Dual-UAV Trajectory and RIS Design for ARIS-Assisted Aerial Computing in IoT," *IEEE IOT J.*, vol. 10, no. 22, pp. 19584-19594, Nov. 2023.

[8] L. Li, W. Guan, C. Zhao, Y. Su, and J. Huo, "Trajectory Planning, Phase Shift Design, and IoT Devices Association in Flying-RIS-Assisted Mobile Edge Computing," *IEEE IOT J.*, vol. 11, no. 1, pp. 147-157, Jan. 2024.

[9] Y. Zeng, R. Zhang, and T. J. Lim, "Wireless communications with unmanned aerial vehicles: opportunities and challenges," *IEEE Commun. Mag.*, vol. 54, no. 5, pp. 36-42, May 2016.

[10] Y. Ma, M. Li, Y. Liu, Q. Wu, and Q. Liu, "Active Reconfigurable Intelligent Surface for Energy Efficiency in MU-MISO Systems," *IEEE Trans. Veh. Technol.*, vol. 72, no. 3, pp. 4103-4107, Mar. 2023.

[11] Z. Yigit, E. Basar, M. Wen, and I. Altunbas, "Hybrid Reflection Modulation," *IEEE Trans. Wireless Commun.*, vol. 22, no. 6, pp. 4106-4116, Jun. 2023.

[12] R. Long, Y. -C. Liang, Y. Pei, and E. G. Larsson, "Active reconfigurable intelligent surface-aided wireless communications," *IEEE Trans. Wireless Commun.*, vol. 20, no. 8, pp. 4962-4975, Aug. 2021.

[13] Y. Du, K. Yang, K. Wang, G. Zhang, Y. Zhao, and D. Chen, "Joint Resources and Workflow Scheduling in UAV-Enabled Wirelessly-Powered MEC for IoT Systems," *IEEE Trans. Veh. Technol.*, vol. 68, no. 10, pp. 10187-10200, Oct. 2019.

[14] H. Mei, K. Yang, Q. Liu, and K. Wang, "3D-Trajectory and Phase-Shift Design for RIS-Assisted UAV Systems Using Deep Reinforcement Learning," *IEEE Trans. Veh. Technol.*, vol. 71, no. 3, pp. 3020-3029, Mar. 2022.

[15] Y. Zeng, J. Xu, and R. Zhang, "Energy Minimization for Wireless Communication With Rotary-Wing UAV," *IEEE Trans. Wireless*, vol. 18, no. 4, pp. 2329-2345, Apr. 2019.